THE JOURNAL OF PHYSICAL CHEMISTRY C

Article

pubs.acs.org/JPCC

Tunable Luminescence in CdSe Quantum Dots Doped by Mn Impurities

Vitaly Proshchenko and Yuri Dahnovsky*

Department of Physics and Astronomy, University of Wyoming, 1000 East University Avenue, Department 3905, Laramie, Wyoming 82071, United States

ABSTRACT: In this work, we study the effect of a dual luminescence for CdSe quantum dots (QDs) doped by a manganese impurity. In this effect, one line has fast relaxation and corresponds to light emission from CdSe conduction band, whereas the second is very slow in relaxation with the relaxation time of 0.1−1.0 ms. The second line disappears for quantum dots (QDs) with diameters $D \geq 3.3$ nm, and therefore, the luminescence becomes tunable by a QD size. The problem is computationally challenging because of large size QDs and a high degeneracy of the energy states. To overcome this problem, we make four assumptions. These assumptions are the following: (1) a QD optical gap is independent of an Mn impurity for small concentrations; (2) we combine electronic structure calculations for medium size CdSe QDs with the effective mass calculations for medium and large QD sizes and match them in the medium size region, assuming that based on assumption 1, the optical spectrum is independent of Mn even for larger QDs; (3) we cut an $MnSe_4$ fragment out of the middle of $Cd_{23}Mn_1Se_{24}$, $Cd_{31}Mn_1Se_{32}$, and $Cd_{81}Mn_1Se_{82}$ QDs and check whether we can quantitatively explain the mechanism of the second, slow relaxation emission in these experiments using the ab initio SAC−CI multiconfiguration method; and (4) the slow luminescence line is independent of a QD size. We have proved theoretically all these assumptions and found that the critical size of a quantum dot, the size when the second luminescence line disappears, is 3.2 nm, and the slow luminescence energy is 2.3 eV in a tetrahedral ligand field. We also study the case for an Mn impurity placed at a QD surface. Then the symmetry of a fragment is C_{3v}, and the results of the calculations reveal that the slow luminescence energy is 2.47 eV with the critical size $D = 2.7$ nm, instead of 3.2 nm for a tetrahedral ligand field. We also predict how this energy depends on the length of an Mn−Se bond. The dependencies appear to be the opposite in these two cases. For the tetrahedral symmetry, the luminescence energy grows with the bond length, whereas for the pyramid, C_{3v}, symmetry (an Mn is at the surface), it goes down. Furthermore, we study a luminescence energy dependence on a Se−Mn−Se pyramid angle. We find that it is angle independent. These results could be useful for CdSe nanocrystal structures different than Würtzite.

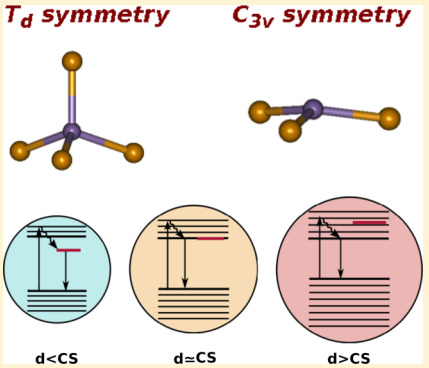

I. INTRODUCTION

Semiconductor nanocrystals, as a class of luminescent chromophores, are important in the growing fields of nanoscience and nanotechnology.[1−36] In spherical dots, band gaps and oscillator strengths can be tuned by variation of the diameter while for quantum rod and tubes by the radii and lengths.[35−37] The incorporation of transition metal (TM) magnetic impurities into a semiconductor lattice can control photoconductivity, alter optical, and change magnetic properties of nanocrystals. TM dopants can be efficient in photovoltaic energy conversion,[38−42] nanospintronics and spin-photonics,[43] magneto optical and magneto-electronic properties,[44−52,54] and the giant Zeeman effect.[55] Photoluminescence properties become unusual if nanocrystals are doped by Mn atoms. In this case, one observes dual or single emission, thus tunable, depending on a $Cd_{n-x}Mn_xSe_n$ quantum dot (QD) size.[43,56−58] The experiments reveal that there are two emission lines for small QDs and a single emission line for larger sizes. If two light transitions take place, the lower energy luminescence lives much longer than the light emission with a lifetime about 0.1−1.0 ms for $Cd_{n-x}Mn_xSe_n$ nanocrystals.[43,56−58] The higher energy line has a short lifetime within a nanosecond range. For larger sizes, the emission lifetime is also short—approximately several nanoseconds. The light emission is schematically shown in Figure 1. The red line stands for the excited state of an Mn atom in a crystals field. Two emission lines are shown by the black arrows. As mentioned above, the long-living emission disappears for larger QDs. This effect has to be explained theoretically. Thus, in this work, we computationally prove the effect of disappearance of the long lifetime emission line at some critical size of a QD. The difficulty of a theoretical description is due to small oscillator strengths, which are 10^6 times smaller than for the fast emission. It is practically impossible to calculate oscillator strengths for such a transition. Such a small oscillator strength is expected because it is forbidden by spin. In reality, the luminescence, nevertheless, takes place due to small spin−orbit interaction as mentioned in refs 43,56−.

In this work, we theoretically study both luminescence lines for an Mn impurity that is placed in the middle and also at the

Received: October 13, 2014
Revised: November 11, 2014
Published: November 12, 2014

   dx.doi.org/10.1021/jp5103324 | J. Phys. Chem. C 2014, 118, 28314−28321

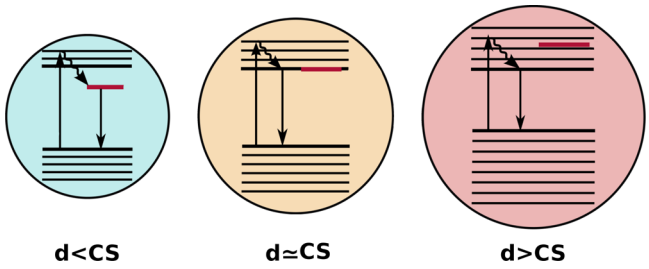

Figure 1. Photoemission of light from the excited electronic state to the ground state in a ligand field. The emission depends on the size of a quantum dot. For a smaller quantum dot, there are two emission lines, and for the intermediate and larger sizes, there is only one emission line. CS stands for a critical size.

surface of a quantum dot, as shown in Figure 2a,b. The ligand field symmetries in both cases are different. If an Mn impurity is located in the middle of a quantum dot, the ligand field symmetry is close to T_d where an excited state has a $^4T_1$ symmetry with the ground state symmetry $^6A_1$. For an Mn impurity placed at a QD surface, the ligand field symmetry is close to C_{3v}, and therefore, a single electron energy picture is different to the case with the tetrahedral geometry. The single electron energy level picture for both symmetries is schematically shown in Figure 3. In this figure, there are two levels where one of them is triply degenerate, although the second is doubly degenerate in the tetrahedral configuration. In C_{3v} symmetry, there are three levels where two of them are doubly degenerate and one is nondegenerate. In the excited state, spin orbitals have ^4E symmetry, whereas for the ground state, it is $^6A_2$. The symmetries of single electronic states are indicated for both cases. The experiments of Gamelin and co-workers state that an Mn impurity is placed in the middle of a QD (case 1).[43,56−58] Case 2, where an Mn impurity is located at a QD surface, has not been experimentally studied; however, the calculations indicate that physical effects are different.

II. COMPUTATION PLAN

In this work we would like to theoretically explain the origin of two luminescence lines taking place in $Cd_{n-x}Mn_xSe_n$ quantum dots.[43,56−58] If one increases a QD size, the second line disappears at the critical diameter, $D \geq 3.3$ nm. For smaller QDs with two luminescence lines, one emission is very fast while the second transition takes place with the much longer relaxation time within 0.1−1.0 ms.[43,56−58] We should also note

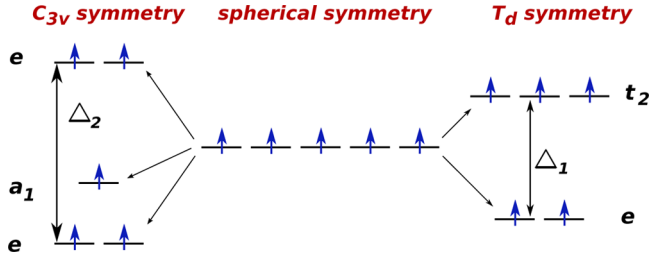

Figure 3. Spherically symmetric 5-fold degenerate level is split in two different ligand fields with T_d symmetry on the right and C_{3v} symmetry on the left.

that the second emission occurs with a spin-flip, and therefore, it is forbidden by spin. Nevertheless, the luminescence still takes place due to a small spin−orbitinteraction. For this emission, $\hbar\omega$ = 2.1−2.2 eV.[43,56−58] The fast luminescence is obviously light emission from the conduction to valence band. As it was suggested by Gamelin and co-workers, it is determined by a CdSe QD only and independent of an Mn impurity at small concentrations.[43,56−58] The second line, however, is determined by an Mn atom surrounded by Se atoms composing a fragment with approximate T_d or C_{3v} symmetries. All these assumptions are not obvious and have to be computationally verified and proved. However, there are several computational problems. First, because of very slow relaxation, the second emission has extremely small oscillator strengths, that is 10^6 times smaller than for the allowed transition in the dipole approximation. Apparently, such an optical transition cannot be calculated even by the fast standard computational methods such as TDDFT, CIS, DFT etc. Second, electronic structure calculations cannot be performed for CdSe QDs doped by Mn atoms with the critical and larger diameters because of large number of atoms in a QD to prove a disappearance of the second, slow emission. Furthermore, an Mn impurity surrounded by Se atoms with T_d or C_{3v} symmetries has degenerate electronic states that cannot be calculated in the single configuration approximation. In this particular case oneshould use multiconfiguration computational methods that appear to be very slow and therefore, cannot be applied to a QD with realistic number of atoms. All these difficulties make this problem unrealistic for electronic structure calculations by modern computational methods.

Nevertheless we believe that these problems can be resolved if one employs some approximations based on a physical picture of the processes taking place. Thus, we propose the

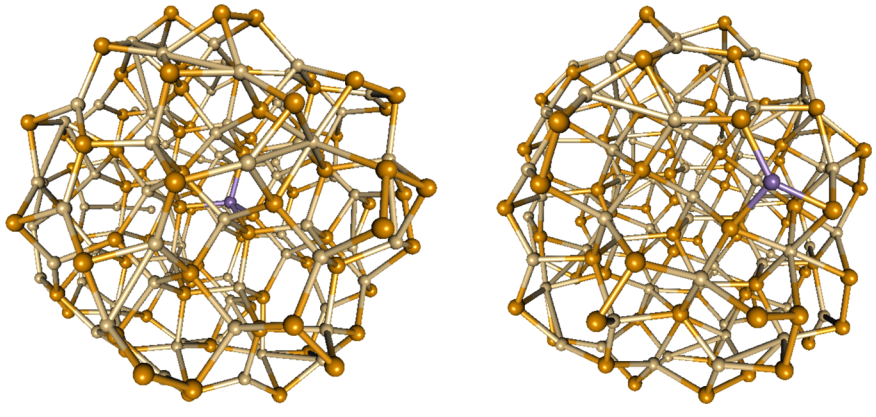

Figure 2. $Cd_{81}Mn_1Se_{82}$ quantum dot where an Mn atom (purple) is placed (a) in the middle and (b) at the surface of a QD.

dx.doi.org/10.1021/jp5103324 | J. Phys. Chem. C 2014, 118, 28314−28321

following plan of calculations that drastically simplifies computations. This plan includes the following approximations that we verify in quantum chemical calculations.

Assumption 1. An Mn impurity does not change an optical gap and therefore, one can study a CdSe QD without Mn atoms for optical gap calculations. This assumption allows us to employ a size dependence of optical gap calculated in the effective mass including exciton effect approximation (see e.g.[7,8,21,22]) for larger QDs.

Assumption 2. As soon as assumption 1 is proved, we conclude that the slow emission transition is due to thepresence of an Mn atom in a CdSe QD. Thus, we cut out ofquantum dots the smallest fragments that include an Mn atom as shown in Figure 4.

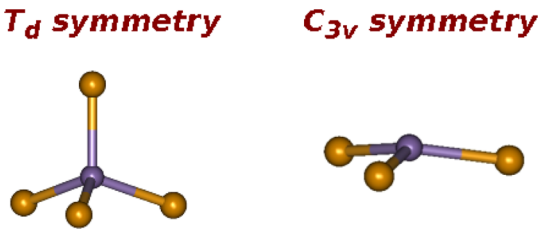

Figure 4. $MnSe_4$ and $MnSe_3$ fragment in T_d and C_{3v} symmetry configurations.

Assumption 3. Since the fragments described in assumption 2 do not possess precise T_d or C_{3v} symmetries, we prove that energy structures and geometry of the fragments are very close to those of with the designated symmetries. For the calculations we use only the symmetric configurations of the fragments because calculations turn out to be much faster in the multiconfiguration approach. In addition, it becomes possible to classify electronic states according to their symmetries.

Assumption 4. It was experimentally observed that a second luminescence line does not depend on a QD size. Thus, it makes us confident that calculations performed for a fragment are valid for larger QDs.[7,8,21,22] We verify this observation in our calculations. We also verify this assumption for a fragment with the C_{3v} symmetry.

III. COMPUTATIONAL DETAILS

Because the calculation plan has been outlined, we specify computation details for each step. To find electronic structures of various quantum dots, we use a Gaussian-09 software package.[60] First, all spherical CdSe QDs were cut out from a Würtzite bulk structure and optimized by the DFT method with a B3LYP exchange-correlation functional and LANL2dz basis set. For the $Cd_{n-x}Mn_xSe_n$ QD geometry optimization, we also use the same method, unrestricted functional and basis set. The optical spectrum calculations for doped and undoped CdSe QDs have been performed by TDDFT. An exchange−correlation functional has been chosen to agree with the calculations by the ab initio CISD method that includes electron correlations. The best fit turns out to be CAM-B3LYP. In Figure 5, we demonstrate how the TDDFT optical spectrum for $(CdSe)_{10}$ fits the CISD curve. The discrepancy between the CISD and TDDFT methods is less than 0.1 eV for the optical spectrum. We have tested several basis sets for Cd and Se: LANL2dz, Stuttgart, and cc-pVDZ; and for Mn: LANL2dz, 6-31G*+, and cc-pVDZ. The choice of a working basis set is based on the two criteria: (a) the maximum agreement with the

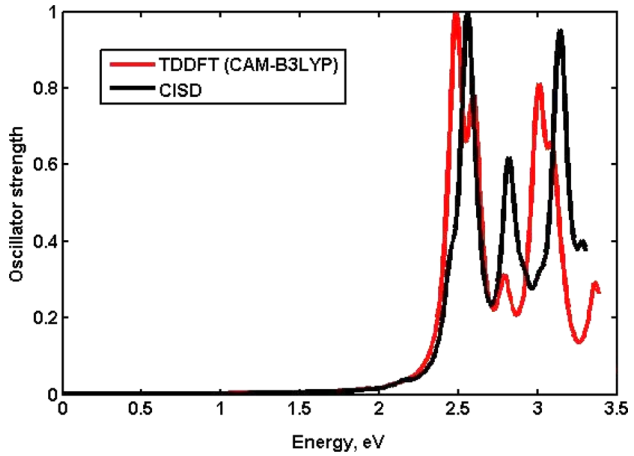

Figure 5. Optical spectrum for $(CdSe)_{10}$ calculated by CISD (black line) and TDDFT (red line).

largest basis set, cc-pVDZ and (b) the shortest time of calculations. Such a basis set has appeared to be a LANL2dz one for Cd and Se atoms, and 6-31G*+ for an Mn atom. The choice of an exchange−correlation functional and basis sets has been employed for $Cd_{10}Se_{10}$ and $Cd_9Mn_1Se_{10}$ QDs. As shown in Figure 6, the optical spectrum has demonstrated almost no

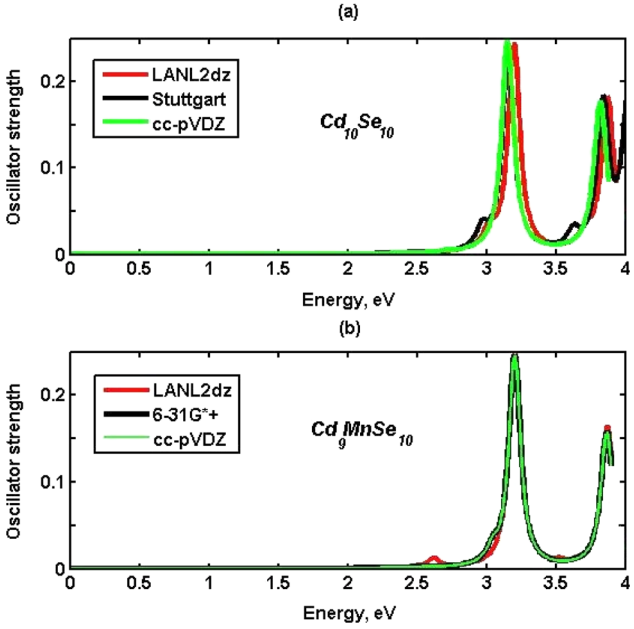

Figure 6. Optical spectra calculated by the CIS method for (a) $(CdSe)_{10}$ with different basis sets: LANL2dz (the red line), Stuttgart (the black line), and cc-pVDZ (the green line) and (b) $Cd_9Mn_1Se_{10}$ with different basis sets for a Mn atom: LANL2dz (the red line), 6-31G*+ (the black line), and cc-pVDZ (the green line).

discrepancy with the CIS calculations if we use (a) LANL2dz, Stuttgart, and cc-pVDZ for Cd and Se in the undoped case and (b) LANL2dz, 6-31G*+, and cc-pVDZ basis sets for a Mn in the doped case. We also employ a LANL2dz basis set for Cd and Se atoms in $Cd_{n-x}Mn_xSe_n$ QDs. For further calculations, we have chosen a LANL2dz basis set for Cd and Se and 6-31G*+ basis set for Mn atoms. In order to calculate optical gaps for large QDs, we use the DFT method with the additional original program[61] that allows us to find oscillator strengths for optical

dx.doi.org/10.1021/jp5103324 | J. Phys. Chem. C 2014, 118, 28314−28321

transitions between unoccupied and occupied states. In this work, we are only interested in the lowest energy transitions that determines an optical gap. For these calculations, we have tried various exchange−correlation functionals: B3LYP, PBEPBE1, CAM-B3LYP, and a LANL2dz basis set. It turned out that the best agreement with the optical gap calculations in the effective mass approximation[7,8,21,22] is provided by a B3LYP exchange−correlation functional.

For $MnSe_4$ and $MnSe_3$ fragment electronic structure calculations, we have considered the multiconfiguration approach provided by the SAC−CI method. The multiconfiguration Slater determinants employ the spin orbitals found from ROHF (Restricted-Open-Shell-Hartree−Fock) calculations. In these calculations, T_d and C_{3v} symmetries have remained unchanged for both ground (M = 6) and excited (M = 4) states. The energy difference between these states determines the luminescence energy for the slow relaxation emission.

IV. RESULTS AND DISCUSSION

In section II, we have laid out the plan of calculations with some assumptions that we prove in this section. These assumptions are necessary because of the impossibility of modern computational resources and methods to do calculations for large size quantum dots with multiconfiguration basis sets. However, some physical observations might be helpful to solve the problem under consideration.

Assumption 1. According to this assumption, we have to verify whether an optical gap of a $Cd_{n-x}Mn_xSe_n$ QD is independent of an Mn impurity. Using only electron structure calculations, we are not able to find a critical QD size for a dual emission disappearance because this size quantum dot is too large. In this case, it would be useful to pay attention to other, more efficient but empirical computational methods such as the effective mass approximation for nanocrystals.[7,8,21,22] This method provides excellent results for large and intermediate size CdSe QDs without Mn doping. If we calculate optical gaps for intermediate size QDs using electronic structure methods and then match them with the optical gaps found in the effective mass approach in the intersection region, then we are confident that both methods work seamlessly for the intermediate and large size QDs but in the case of Mn doping. In Figure 7, we demonstrate how the optical spectrum depends on the presence of an Mn impurity. From this figure, we conclude that the optical spectrum remains almost unchanged in the presence of the Mn atom. There is a small deviation for the impurity placed at a QD surface. If the impurity is in the middle of a quantum dot, the spectra are almost indistinguishable. In Figure 7, we have taken $Cd_{16}Se_{16}$ and $Cd_{15}Mn_1Se_{16}$ quantum dots. To make sure that the optical gap is independent of doping for different size QDs, we have performed the same calculations but for the larger QDs, $Cd_{24}Se_{24}$, and $Cd_{23}Mn_1Se_{24}$, and we have shown that the gap is the same in the absence and presence of the Mn impurity. We have done the calculations for Mn placed in the middle and at the surface of a quantum dot. The computations have been performed with the TDDFT method with a LANL2dz basis set where the exchange correlation functional have been adjusted to the CISD results, as described in Figure 5. We have not presented $Cd_{24}Se_{24}$ and $Cd_{23}Mn_1Se_{24}$ QD calculations in the figure because they have the same picture proving that the optical spectra are independent of the presence of an Mn impurity. Thus, we conclude that assumption 1 has been proved.

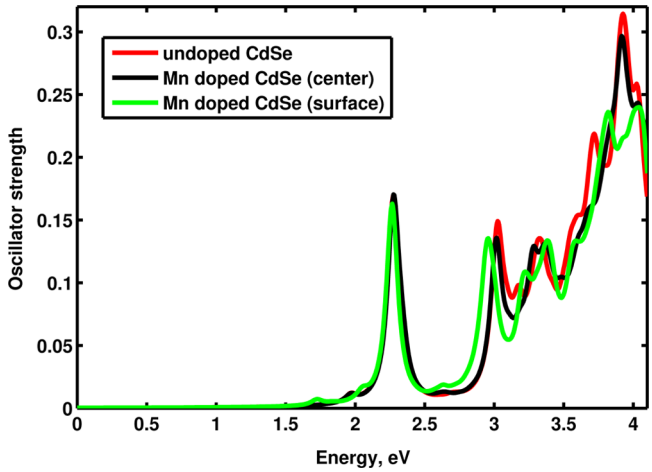

Figure 7. Optical spectra for $Cd_{16}Se_{16}$ (the red line) and $Cd_{15}Mn_1Se_{16}$ with an Mn impurity in the middle of a QD (black) and at a QDsurface (green). The calculations are performed within the TDDFT method with the CAM-B3LYP exchange-correlation functional.

Assumption 2. As soon as assumption 1 is proved, we are able now to calculate electronic structures for intermediate size quantum dots but doped by Mn atoms. We know now that an Mn impurity does not affect the optical gap, but rather, it determines the slow relaxation luminescence. Assumption 2 states that instead of QD calculations with an Mn atom for intermediate sizes, we can cut out fragments—$MnSe_4$ with close to T_d and $MnSe_3$ to C_{3v} symmetries—with geometries and energy levels that are independent of a QD size. Moreover, if we extend this approximation to larger size QDs, an energy levels of a fragment remain the same compare to the results found for the intermediate size QDs from the electronic structure calculations. The optical gaps calculated in the effective mass approximation[7,8,21,22] for large and intermediate QD sizes are presented by the black solid line shown in Figure 8. We have calculated optical gaps for the different size QDs such as $Cd_{24}Se_{24}$, $Cd_{32}Se_{32}$, and $Cd_{82}Se_{82}$ by DFT in conjunction with the additional original program that allows us to find oscillator strengths.[61] The exchange−correlation

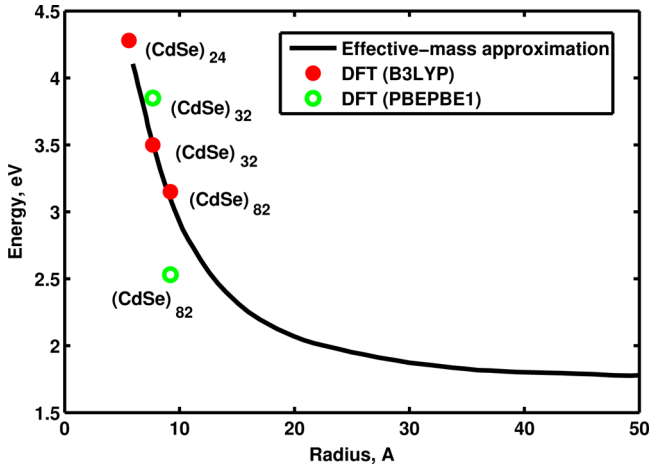

Figure 8. Size dependence of optical gap for CdSe QDs calculated in the effective-mass approximation (the black line), DFT with B3LYP (the red dots, and PBEPBE1 (the green dots) exchange−correlation functionals.

dx.doi.org/10.1021/jp5103324 | J. Phys. Chem. C 2014, 118, 28314−28321

functional has been selected in a way that the values of optical gaps have to match the ones predicted in the effective mass approximation. In Figure 8, we demonstrate the calculations of optical gaps employing the B3LYP (red) and PBEPBE1 (green) exchange−correlation functionals. It becomes clear that the results found with B3LYP provides the better match to the effective mass optical gaps. We have also tested CAM-B3LYP exchange−correlation functional (it is not shown in Figure 8) where the values of optical gaps are too far from the effective mass approximation predictions. Thus, doped by manganese, $Cd_{24}Se_{24}$, $Cd_{32}Se_{32}$, and $Cd_{82}Se_{82}$ QDs can be safely used for further calculations, making sure that gap values are unaffected by an Mn impurity for larger size QDs.

Assumption 3. The next step is to cut an $MnSe_4$ for T_d and $MnSe_3$ for C_{3v} fragments out of the three QDs of different sizes: $Cd_{23}Mn_1Se_{24}$, $Cd_{31}Mn_1Se_{32}$, and $Cd_{81}Mn_1Se_{82}$. As shown in Figure 9 single electron energy states are almostunchanged and

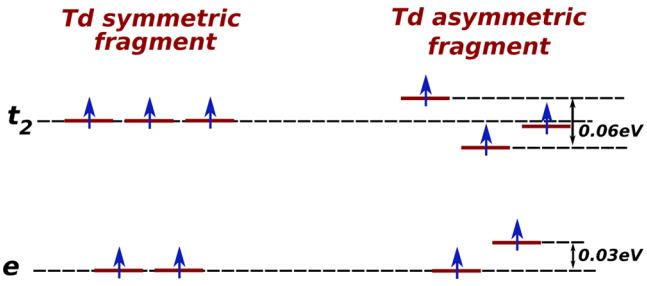

Figure 9. Single electron energy states for symmetric and asymmetric T_d fragment cut out from $Cd_{31}Mn_1Se_{32}$.

independent of a QD size. The calculations have been performed by DFT with the UB3LYP exchange−correlation functional. In Figure 9, we also demonstrate a tetrahedral symmetry fragment (see Figure 4) with the energy levels close to the ones for real asymmetric cut. For the T_d fragment, three t_2 single electron levels are degenerate while the lower e^- single electron state is doubly degenerate.[59] We have found that the discrepancy between t_2 levels in the asymmetric fragment is about 0.06 eV, and for e-levels, it is only 0.03 eV. The calculations presented above make us confident that we can use now a T_d symmetric fragment for the further calculations. The same type of calculations we performed for the C_{3v} fragment show negligible energy differences between symmetric and asymmetric fragments. In C_{3v} symmetry, there are three levels where two of them are doubly degenerate (e-levels) and one is nondegenerate (an a_1 level). Now we are ready to find energy states for the symmetric fragment. In these calculations, we are interested in the ground state with the symmetry $^6A_1$ (M = 6) and the excited one with the symmetry $^4T_1$ (M = 4) for the tetrahedral ligand field and the ground state with $^6A_2$ (M = 6) and the excited state with ^4E (M = 4) symmetries for C_{3v} ligand field. For the excited states in both symmetries, we imply that a spin of one electron is flipped. Because of the high degeneracy of the single electron states, we have to use a calculation method that includes a multiconfiguration basis set. For this purpose, we have chosen the SAC−CI method. In the SAC−CI calculations, we keep the T_d or C_{3v} symmetries of the fragments unchanged during the computations. The Slater determinants for a basis set are built up from the spin orbits found from the restricted open shell Hartree−Fock calculations. These calculations reveal that the energy difference between the excited (M = 4) and ground (M = 6) states is 2.3 eV for the T_d symmetric fragment cut out of the $Cd_{31}Mn_1Se_{32}$ QD. For the C_{3v} fragment, we have obtained ΔE = 2.47 eV. Both transition are allowed in the dipole approximation but forbidden by spin. The energy transition for C_{3v} fragment is the prediction.

Assumption 4. We have also calculated the electronic structures for two other size QDs and found that the slow luminescence energies still remain unchanged. Because it has been proved that the energy difference ΔE is the same for intermediate size QDs, we can safely assume that the same value of ΔE stays for the larger size QDs (see Figure 8).

Because optical gaps are independent of Mn doping (assumption 1) and the energy of the slow luminescence is also independent of a QD size, we can easily find from the crossing of these two curves the critical sizes for both symmetries, as shown in Figure 10. The critical size is defined

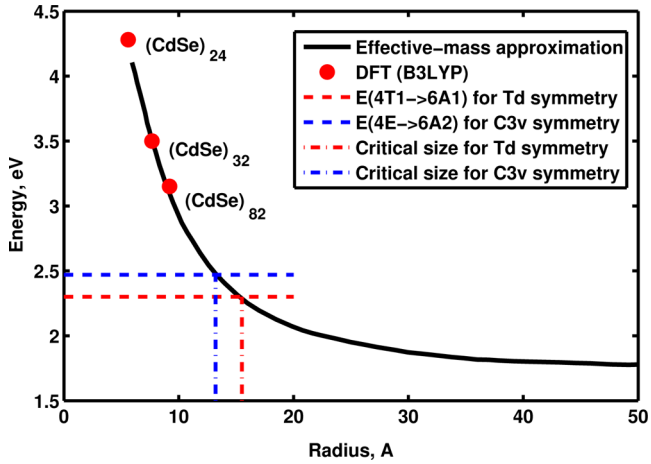

Figure 10. Crossing points between the energy differences ΔE and the optical gap curve from Figure 8 determines the critical size for a QD ($D \simeq 3.2$ nm for T_d and $D \simeq 2.7$ nm for C_{3v} crystal ligand symmetries, respectively) where the slow relaxation luminescence disappears from the emission spectrum.

by a condition where a slow relaxation emission line disappears from the luminescence spectrum. The crossing point between the line with ΔE = 2.3 eV and the optical gap curve determines the critical size QD diameter D = 3.2 nm for a Mn impurity placed in the middle of the quantum dot. This result confirms the experimental value of 3.3 nm, which was found by Gamelin and co-worker in refs 43,56−58. If an impurity is located at a QD surface, the critical size is $D \simeq 2.7$ nm. The critical sizes for both fragment symmetries are presented in Figure 10.

For future experiments, it is interesting to predict how the energy difference ΔE depends on the length of a Mn−Se chemical bond and angle between Mn−Se and Mn−Se chemical bonds in the C_{3v} pyramid. In Figure 11, we demonstrate such a dependence for a T_d symmetric fragment (a blue line). The longer the chemical bond, the larger the ΔE. If the fragment has C_{3v} symmetry, the dependence is the opposite—the larger the bond length, the smaller the low luminescence energy. These two lines cross at L = 2.62 Å. We have also studied the luminescence energy depending on the Se−Mn−Se angle in a pyramid with the C_{3v} symmetry for the fragment places at a QD surface, as shown in Figure 12. We have found that the slow luminescence energy is insensitive to the angle. The angle of 120° corresponds to a degenerate case when the pyramid descends to a plane triangle with the D_3 symmetry. Such theoretical dependences can be useful if one

dx.doi.org/10.1021/jp5103324 | J. Phys. Chem. C 2014, 118, 28314−28321

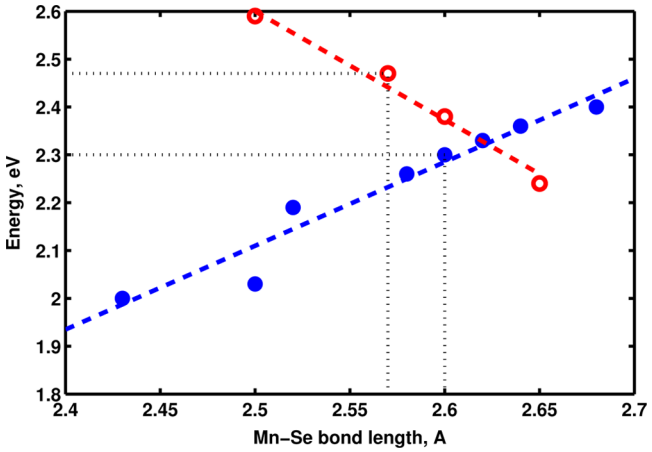

Figure 11. Energy difference ΔE dependence on a Mn−Se bond length. For Mn−Se, bond length = 2.6 Å, and the ΔE = 2.3 eV for the tetrahedral ligand field. The red line represents an energy difference dependence for a fragment having C_{3v} symmetry.

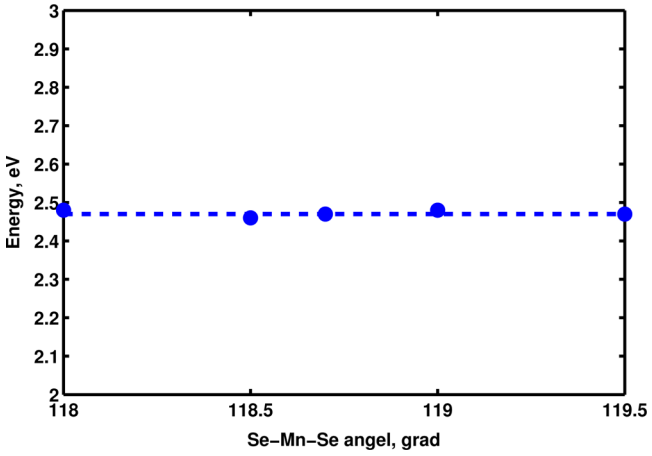

Figure 12. Energy difference ΔE dependence on a Se−Mn−Se angle for a fragment having C_{3v} symmetry.

studies different Würtzite nanocrystal structures corresponding to different bond lengths and pyramid angles.

V. CONCLUSIONS

In this work, we have theoretically studied a dual luminescence effect taking place in CdSe quantum dots doped by a manganese impurity. Experimentally, dual luminescence was discovered by Gamelin and co-workers[43,56−58] where two emission lines took place; one emission is fast, while the second is slow with the relaxation time of 0.1−1.0 ms. The second, slow emission line disappears from the spectrum at some critical QD size, and then only a single emission survives at larger size QDs. Thus, the luminescence becomes tunable. The difficulty in the explanation of the effect is based on a very small oscillator strength, that is about 10^6 times lesser than a usual dipole oscillator strength. Therefore, it becomes impossible to calculate an optical spectrum within the conventional computation methods. The other reason that makes this problem even more computationally difficult is a high degeneracy of energy states. Indeed, the five degenerate levels in a spherical symmetry are split in two levels in a tetrahedral ligand field where the highest level is triply degenerate while the lowest is doubly degenerate. If an impurity is located at a QD surface, the 5-fold degenerate level is split in three levels in a C_{3v} ligand field where two of the levels are doubly degenerate (see Figure 9). Thus, this problem becomes computationally challenging because the standard computational methods such as DFT, TDDFT, CIS, among others, use a single Slater determinant basis set. The theory recommends employing a multiconfiguration basis set. To explain the experimental dependencies,[43,56−58] we have proposed a computational scheme where we have made the four assumption. These assumptions are the following: (1) QD optical gaps are independent of an Mn impurity at small concentrations; (2) we combine electronic structure calculations for medium size CdSe QDs with the effective mass calculations for medium and large size QDs and match them in the medium size intersection region, assuming that based on assumption 1, the optical spectrum is independent of Mn even for larger QDs; (3) we cut an $MnSe_4$ fragment out of $Cd_{23}Mn_1Se_{24}$, $Cd_{31}Mn_1Se_{32}$, and $Cd_{81}Mn_1Se_{82}$ QDs and check whether electronic structures of these fragments explain the second, slow relaxation emission in the experiments; and (4) the slow luminescence line is independent of a QD size. We should note here that these assumptions were also made for the interpretation of the results in refs 43,56−58. In addition, we also consider an Mn impurity located at a QD surface. In this case, the symmetry becomes C_{3v}. The results of these calculations are the predictions. We have computationally proved that all assumptions are correct for both symmetries. According to the calculations, we have proved assumption 1. The results are presented in Figure 7, where we have found that the optical gaps for $Cd_{16}Se_{16}$ (the red line) and $Cd_{15}Mn_1Se_{16}$ QDs with an Mn impurity are independent of Mn at small concentrations. Then we have proved assumption 2. We have tried several exchange−correlation functionals for DFT to match the optical gap size dependence found in the effective mass approximation for large and intermediate size CdSe QDs.[7,8,21,22] Such an approach allows us to do calculations with an Mn impurity for intermediate size QDs and extend them to larger sizes using the effective mass approximation for doped QDs. The results of the computations are presented in Figure 8, where we have found that a B3LYP functional provides the best fit. To prove assumption 3, we have cut an $MnSe_4$ fragment out of the three QDs of different sizes: $Cd_{23}Mn_1Se_{24}$, $Cd_{31}Mn_1Se_{32}$, and $Cd_{81}Mn_1Se_{82}$ and found that the slow luminescence energies are independent of a QD size. The same conclusions are true if a fragment is cut out of the surface. These results can be extended to the larger sizes in accordance with assumption 2 within the effective mass approximation, as shown in Figure 8. The asymmetric and symmetric versions of the fragments provide a very close single electron energy levels, as demonstrated in Figure 9. In this case, the electronic structure calculations for symmetric tetrahedral and pyramid fragments have been performed by the SAC−CI method. The calculations reveal that the energy difference between the excited (M = 4) and ground (M = 6) states is 2.3 eV for the tetrahedral symmetric fragment cut out of the $Cd_{31}Mn_1Se_{32}$ QD. This result confirms the experimental value that is 2.1−2.2 eV.[43,56−58] The predicted slow luminescence energy for a configuration when an Mn impurity is placed at the surface is higher than for the tetrahedral ligand field with $\Delta E \simeq 2.47$ eV. We have also found the QD critical size, at which the second emission line disappears. This size is 3.2 nm, as determined by the calculations. The experimental value is 3.3 nm[43,56−58] (Figure 10). For the fragment with the C_{3v} symmetry, the

dx.doi.org/10.1021/jp5103324 | J. Phys. Chem. C 2014, 118, 28314−28321

critical size is smaller (i.e., $D \simeq 2.7$ nm). In addition, we have made some predictions for a critical size dependence with a length of an Mn−Se chemical bond, as shown in Figure 11. For two different Mn geometries, the dependences are very different. In the case of T_d symmetry, the longer the Mn−Se chemical bond, the larger the slow luminescence energy. In the case of C_{3v} symmetry (Mn is at the surface), the luminescence energy decreases with the bond length. We have also studied the luminescence energy dependence with a pyramid angle, Se−Mn−Se. We have found this energy to be angle independent, as shown in Figure 12. These predictions could be useful for a different CdSe nanocrystal structure rather than Würtzite.

AUTHOR INFORMATION

Corresponding Author

*E-mail: yurid@uwyo.edu.

Notes

The authors declare no competing financial interest.

ACKNOWLEDGMENTS

This work was supported by grant no. DEFG02-10ER46728 from the Department of Energy to the University of Wyoming and the University of Wyoming School of Energy Resources through its Graduate Assistantship program.

REFERENCES

(1) Alivisatos, A. P. Semiconductor Clusters, Nanocrystals, and Quantum Dots. *Science* **1996**, *271*, 933−937.

(2) Brus, L. E. Quantum Crystallites and Nonlinear Optics. *Appl. Phys. A: Mater. Sci. Process.* **1991**, *53*, 465−474.

(3) Akimov, A. V.; Neukirch, A. J.; Prezhdo, O. V. Theoretical Insights Into Photoinduced Charge Transfer and Catalysis at Metal Oxide Surfaces. *Chem. Rev.* **2013**, *113*, 4496−4565.

(4) Gleiter, H. Nanostructured Materials. *Adv. Mater.* **1992**, *4*, 474−481.

(5) Lehmann, V.; Gosele, U. Porous Silicon: Quantum Sponge Structures Grown by a Self-Adjusting Etching Process. *Adv. Mater.* **1992**, *4*, 114−116.

(6) Sailor, M. J.; Kavanagh, K. L. Porous Silicon-What is Responsible for the Visible Luminescence? *Adv. Mater.* **1992**, *4*, 432−4.

(7) Efros, A. L.; Efros, A. L. Interband Absorption of Light in Semiconductor Sphere. *Sov. Phys.-Semicond.* **1982**, *16*, 772−775.

(8) Efros, A. L.; Kharchenko, V. A.; Rosen, M. Breaking the Phonon Bottleneck in Nanometer Quantum Dotsrole of Auger-Like Process. *Solid State Commun.* **1995**, *93*, 281−284.

(9) Brus, L. E. A Simple Model for the Ionization Potential, Electron Affinity, and Aqueous Redox Potentials of Small Semiconductor Crystallites. *J. Chem. Phys.* **1983**, *79*, 5566−5571.

(10) Rossetti, R.; Ellison, J. L.; Gibson, J. M.; Brus, L. E. Size Effects in the Excited Electronic States of Small Colloidal CdS Crystallies. *J. Chem. Phys.* **1984**, *80*, 4464−4469.

(11) Weller, H.; Koch, U.; Gutierrez, M.; Henglein, A. Photochemistry of Colloidal Metal Sulfides. *Ber. Bunsenges. Phys. Chem.* **1984**, *88*, 649−656.

(12) Fojtik, A.; Weller, H.; Koch, U.; Henglein, A. Photochemistry of Colloidal Metal Sulfides. *Ber. Bunsenges. Phys. Chem.* **1984**, *88*, 969−977.

(13) Brus, L. E. Zero Dimensional Excitons inSemiconductor Clusters. *IEEE J. Quantum Electron.* **1986**, *22*, 1909.

(14) Henglein, A. Mechanism of Reactions on Colloidal Microelectrodes and Size Quantization Effects. *Top. Curr. Chem.* **1988**, *143*, 113−180.

(15) Henglein, A. Small-Particle Research: Physicochemical Properties of Extremely Small Colloidal Metal and Semiconductor Particles. *Chem. Rev.* **1989**, *89*, 1861−1873.

(16) Brus, L. E. Quantum Crystallites and Nonlinear Optics. *J. Appl. Phys. A* **1991**, *53*, 465−474.

(17) Wang, Y.; Herron, N. Nanometer-Sized Semiconductor Clusters: Materials Synthesis, Quantum Size Effects, and Photophysical Properties. *J. Phys. Chem.* **1991**, *95*, 525−532.

(18) Henglein, A. Chemistry and Optical Properties of Small Metal Particles in Aqueous Solution. *MRS Proceedings* **1992**, DOI: 10.1021/cr00098a010.

(19) Weller, H. Kolloidale Halbleiter-Q-Teilchen: Chemie im Ubergangsbereich zwischen Festkorper und Molekul. *Angew. Chem.* **1993**, *105*, 43−55.

(20) Banyai, L.; Koch, S. W. *Semiconductor Quantum Dots*; World Scientific: Singapore, 1993; Vol. 2.

(21) Yoffe, A. D. Low-Dimensional Systems: Quantum Size Effects and Electronic Properties of Semiconductor Microcrystallites (Zero-Dimensional Systems) and Some Quasi-Two-Dimensional Systems. *Adv. Phys.* **1993**, *42*, 173−262.

(22) Yoffe, A. D. Semiconductor Quantum Dots and Related Systems: Electronic, Optical, Luminescence and Related Properties of Low Dimensional Systems. *Adv. Phys.* **2001**, *50*, 1−208.

(23) Piryatinski, A.; Velizhanin, K. A. An Exciton Scattering Model for Carrier Multiplication in Semiconductor Nanocrystals: Theory. *J. Chem. Phys.* **2010**, *133*, 084508−084519.

(24) Kilina, S.; Velizhanin, K. A.; Ivanov, S.; Prezhdo, O. V.; Tretiak, S. Surface Ligands Increase Photoexcitation Relaxation Rates in CdSe Quantum Dots. *ACS Nano* **2012**, *6*, 6515−6524.

(25) Kilina, S.; Kilin, D.; Prezhdo, V. V.; Prezhdo, O. V. Theoretical Study of Electron-Phonon Relaxation in PbSe and CdSe Quantum Dots: Evidence for Phonon Memory. *J. Phys. Chem. C* **2011**, *115*, 21641−21651.

(26) Prezhdo, O. V. Photoinduced Dynamics in Semiconductor Quantum Dots: Insights from Time-Domain ab Initio Studies. *Acc. Chem. Res.* **2009**, *42*, 2005−2016.

(27) Neukrich, A. J.; Hyeon-Deuk, K.; Prezhdo, O. V. Time-Domain ab Initio Modeling of Excitation Dynamics inQuantum Dots. *Coord. Chem. Rev.* **2014**, *263*, 161−181.

(28) Kilina, S. V.; Kilin, D. S.; Prezhdo, O. V. Breaking the Phonon Bottleneck in PbSe and CdSe Quantum Dots: Time-Domain Density Functional Theory of Charge Carrier Relaxation. *ACS Nano* **2009**, *3*, 93−99.

(29) Kilina, S. V.; Craig, C. F.; Kilin, D. S.; Prezhdo, O. V. Ab Initio Time-Domain Study of Phonon-Assisted Relaxation of Charge Carriers in a PbSe Quantum Dot. *J. Phys. Chem. C* **2007**, *111*, 4871−4878.

(30) Kilina, S. V.; Neukirch, A. J.; Habenicht, B. F.; Kilin, D. S.; Prezhdo, O. V. Quantum Zeno Effect Rationalizes the Phonon Bottleneck in Semiconductor Quantum Dots. *Phys. Rev. Lett.* **2013**, *110*, 180404−6.

(31) Kilina, S. V.; Ivanov, S.; Klimov, V. I.; Tretiak, S. Effect of Surface Ligands on Optical and Electronic Spectra of Semiconductor Nanoclusters. *J. Am. Chem. Soc.* **2009**, *131*, 7717−7726.

(32) Fischer, S. V.; Crotty, A. M.; Kilina, S. V.; Ivanov, S. A.; Tretiak, S. Passivating Ligand and Solvent Contributions to the Electronic Properties of Semiconductor Nanocrystals. *Nanoscale* **2012**, *4*, 904−914.

(33) Nguyen, K. A.; Pachter, R.; Day, P. R. Computational Prediction of Structures and Optical Excitations for Nanoscale Ultrasmall ZnS and CdSe Clusters. *Chem. Theory Comput.* **2013**, *9*, 3581−3596.

(34) Proshchenko, V.; Dahnovsky, Yu. Size-dependent Density of State and Optical Spectra of Quantum Rods andTubes. *Chem. Phys. Lett.* **2014**, *595*, 250−255.

(35) Proshchenko, V.; Dahnovsky, Yu. Spectroscopic and Electronic Structure Properties of CdSe Nanocrystals: Spheres and Cubes. *Phys. Chem. Chem. Phys.* **2014**, *16*, 7555−61.

(36) Pimachev, A.; Dahnovsky, Yu. Electronic Structure Calculations of PbS Quantum Rods and Tubes. *J. Appl. Phys.* **2014**, *115*, 043705−6.

(37) Hu, J.; Li, L.; Yang, W.; Manna, L.; Wang, L.-W.; Alivisatos, A. P. Linearly Polarized Emission from Colloidal Semiconductor Quantum Rods. *Science* **2001**, *292*, 2060−2063.

(38) Serpone, N.; Lawless, D.; Disdier, J.; Hermann, J. M. Spectroscopic, Photoconductivity, and Photocatalytic Studies of TiO2 Colloids: Naked and with the Lattice Doped with Cr3+, Fe3+, and V5+ Cations. *Langmuir* **1994**, *10*, 643−652.
(39) Kudo, A.; Sekizawa, M. Photocatalytic H2 Evolution Under Visible Light Irradiation on Ni-Doped ZnS Photocatalyst. *Chem. Commun.* **2000**, 1371−1372.
(40) Jaramillo, T. F.; Baek, S.-H.; Kleiman-Shwarsctein, A.; Choi, K.-S.; Stucky, G. D.; McFarland, E. W. Automated Electrochemical Synthesis andPhotoelectrochemical Characterization of Zn1-xCoxO Thin Films for Solar Hydrogen Production. *J. Comb. Chem.* **2005**, *7*, 264−271.
(41) Liu, W. K.; Sally, G. M.; Gamelin, D. R. Spectroscopy of Photovoltaic and Photoconductive Nanocrystalline Co2+-doped ZnO Electrodes. *J. Phys. Chem. B* **2005**, *109*, 14486−14495.
(42) Osterloh, F. E. Inorganic Materials as Catalysts for Photochemical Splitting of Water. *Chem. Mater.* **2008**, *20*, 35−54.
(43) Beaulac, R.; Archer, P. L.; Ochsenbein, S. T.; Gamelein, D. R. Mn2+-Doped CdSe Quantum Dots: New Inorganic Materials for Spin-Electronics and Spin-Photonics. *Adv. Funct. Mater.* **2008**, *18*, 3873−3891.
(44) Norris, D. J.; Yao, N.; Charnock, F. T.; Kennedy, T. A. High-Quality Manganese-Doped ZnSe Nanocrystals. *Nano Lett.* **2001**, *1*, 3−7.
(45) Hoffman, D. M.; Meyer, B. K.; Ekimov, A. I.; Merkulov, I. A.; Efros, Al.L.; Rosen, M.; Counio, G.; Gacoin, T.; Boilot, J. P. Giant Internal Magnetic Fields in Mn Doped Nanocrystal Quantum Dots. *Solid State Commun.* **2000**, *114*, 547−550.
(46) Radovanovic, P. V.; Gamelin, D. R. MagneticCircular Dichroism Spectroscopy of Co2+:CdS Diluted Magnetic Semiconductor Quantum Dots. *Proc. SPIE Int. Soc. Opt. Eng.* **2002**, *4809*, 51−61.
(47) Schwartz, D. A.; Norberg, N. S.; Nguyen, Q. P.; Parker, J. M.; Gamelin, D. R. Magnetic Quantum Dots: Synthesis, Spectroscopy, and Magnetism of Co2+- and Ni2+-Doped ZnO Nanocrystals. *J. Am. Chem. Soc.* **2003**, *125*, 13205−13218.
(48) Norberg, N. S.; Kittilstved, K. R.; Amonette, J. E.; Kukkadapu, R. K.; Schwartz, D. A.; Gamelin, D. R. Synthesis of Colloidal Mn2+:ZnO Quantum Dots and High-TC Ferromagnetic Nanocrystalline Thin Films. *J. Am. Chem. Soc.* **2004**, *126*, 9387−9398.
(49) Norberg, N. S.; Gamelin, D. R. Giant Zeeman Effects in Colloidal Diluted Magnetic Semiconductor Quantum Dots with Homogeneous Dopant Speciation. *J. Appl. Phys.* **2006**, *99*, 08M104−3.
(50) Norberg, N. S.; Dalpian, G. M.; Chelikowsky, J. R.; Gamelin, D. R. Energetic Pinning of Magnetic Impurity Levels in Quantum Confined Semiconductor Nanocrystals. *Nano Lett.* **2006**, *6*, 2887−2892.
(51) Norberg, N. S.; Parks, G. L.; Salley, G. M.; Gamelin, D. R. Giant Excitonic Zeeman Splittings in Colloidal Co2+-Doped ZnSe Quantum Dots. *J. Am. Chem. Soc.* **2006**, *128*, 13195−13203.
(52) Archer, P. I.; Santangelo, S. A.; Gamelin, D. R. Inorganic Cluster Syntheses of TM2+-Doped Quantum Dots (CdSe, CdS, CdSe/CdS): Physical Property Dependence on Dopant Locale. *J. Am. Chem. Soc.* **2007**, *129*, 9808−9818.
(53) Archer, P. I.; Santangelo, S. A.; Gamelin, D. R. Direct Observation of sp−d Exchange Interactions in Colloidal Mn2+- and Co2+-Doped CdSe Quantum Dots. *Nano Lett.* **2007**, *7*, 1037−1043.
(54) Bussian, D. A.; Crooker, S. A.; Yin, M.; Brynda, M.; Efros, Al.L.; Klimov, V. I. Tunable Magnetic Exchange Interactions in Manganese-Doped Inverted Core-Shell ZnSe-CdSe Nanocrystals. *Nat. Mater.* **2009**, *8*, 35−40.
(55) Furdyna, J. K.; Kossut, J. Diluted Magnetic Semiconductors. In *Semiconductors and Semimetals*; Willardson, R. K., Beer, A. C., Eds.; Academic Press: New York, 1988; Vol. 25.
(56) Beaulac, R.; Archer, P. I.; Liu, X.; Lee, S.; Salley, G. M.; Dobrowolska, M.; Furdyna, J. K.; Gamelin, D. R. Spin-Polarizable Excitonic Luminescence in Colloidal Mn2+-Doped CdSe Quantum Dots. *Nano Lett.* **2008**, *8*, 1197−1201.
(57) Vlaskin, V. A.; Jansen, N.; Rijsset, J.; Beaulac, R.; Gamelin, D. Tunable Dual Emission in Doped Semiconductor Nanocrystals. *Nano Lett.* **2010**, *10*, 3670−3674.
(58) Beaulac, R.; Ochsenbein, S. T.; Gamelin, D. *Nanocrystals Quantum Dots*; Klimov, V., Ed.; CRC Press: New York, 2010; pp 397−453.
(59) Cotton, F. A. *Chemical Applications of Group Theory*, 3rd ed.; Wiley-Interscience: New York, 1990; Chapter 9.
(60) Frisch, M. J.; Trucks, G. W.; Schlegel, H. B.; Scuseria, G. E.; Robb, M. A.; Cheeseman, J. R.; Scalmani, G.; Barone, V.; Mennucci, B.; Petersson, G. A. et al. *Gaussian 09*, revision D.01; Gaussian, Inc.: Wallingford CT, 2009.
(61) Pimachev, A. *DFT transition dipole moment and oscillator strength program*; University of Wyoming: Laramie, Wyoming,2013.